ELSEVIER

Dynamics of Atmospheres and Oceans 27 (1997) 383–412

dynamics of atmospheres and oceans

# Tropical–middle latitude interactions viewed via wave energy flux in the frequency domain

T.N. Krishnamurti *, M.C. Sinha, Vasubandhu Misra, O.P. Sharma

*Department of Meteorology, Florida State University, Tallahassee, FL 32306-3034, USA*

Received 6 May 1996; revised 2 July 1996; accepted 29 July 1996

**Abstract**

Over the upper troposphere of the polar latitudes the zonal flows exhibit a large variance on the time scale of the Madden–Julian oscillation, i.e. roughly 30–50 days. The other prominent regions for these intraseasonal oscillations are the Asian and Australian monsoon belts. These two regions are separated by the so-called critical latitude, to the south of which easterlies generally prevail and westerlies are prevalent to the north. A perplexing issue is that of possible tropical–middle latitude interactions across the critical latitude. The notion of the critical latitude emerged from the linear theories for the wave energy flux which assume a constancy in time for the zonal flows. This same problem, viewed in its full non-linear context, can be cast in a frequency domain. Such a formulation does not assume a constancy of the zonal flows in time but does permit the intraseasonal variations of the zonal flows to be present. The computation of the wave energy flux, from the more complete non-linear system in the frequency domain, requires the handling of linear, quadratic and triple product terms via use of Hayashi's co-spectral method. These results of the present study, based on 6 years of daily global data sets, show that wave energy flux clearly passes from the latitudes of the monsoon to the polar latitudes. A strong convergence of wave energy flux in the polar latitudes suggests the tropical–middle latitude convergence interactions across the so-called critical latitude—when the problem is viewed in the frequency domain.


## 1. Introduction

This paper addresses the issue of the maintenance of an upper tropospheric middle latitude maxima in the variance in the intraseasonal oscillations on the Madden–Julian time scale. Krishnamurti and Gadgil (1985) used a year-long FGGE data set, produced by the European Center for Medium Range Weather Forecasts (ECMWF), to examine

* Corresponding author.

0377-0265/97/$17.00 
*PII* S0377-0265(97)00021-3

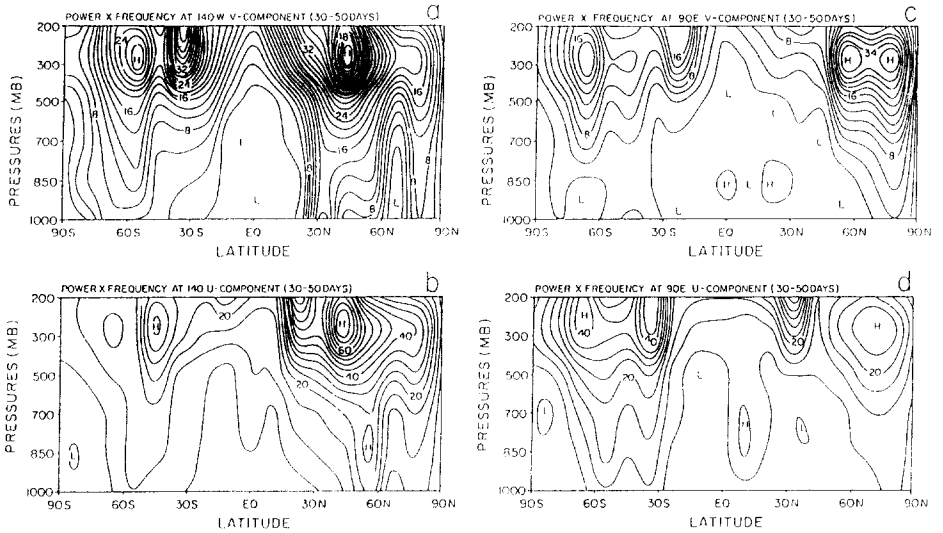


Fig. 1. Latitude–pressure plots of the power spectra (power times the frequency) of the zonal and the meridional wind components at 140°W and 90°E longitude. (a) At 140°W for the meridional wind; (b) at 140°W for the zonal wind; (c) at 90°E for the meridional wind; (d) at 90°E for the zonal wind. These are based on Krishnamurti and Gadgil (1985).

the three-dimensional distribution of these variances. The power spectra of the zonal and the meridional winds shown in Fig. 1(a)–(d) were constructed following the method of Zangvil (1977). Fig. 1(a) illustrates the power spectra over a meridional cross-section for the meridional and the zonal wind at 140°W longitude. Fig. 1(c) and (d) display the power spectra along 90°E. The salient features in these power spectra are the upper tropospheric maxima in the middle and higher latitudes. The monsoonal maxima of the intraseasonal oscillation, noted around 10°N in Fig. 1(d), has been a subject of numerous studies. The maximum over the upper troposphere of the polar latitudes has not been studied adequately. One of the central questions we ask here is: What relationships exist between these monsoonal and the middle latitude maxima (in the variances) on the Madden–Julian time scales (Fig. 1(a)–(d))?

If wave energy flux emanating from the monsoon converges at these high latitudes then the issue of flux across the critical latitude needs addressing. It turns out that the non-linear problem of the wave energy flux in the frequency domain does not face the issue of the critical latitude in the same manner as the linear problem. Furthermore, there exists a robust picture of wave energy flux convergence in the frequency domain that portrays a clear tropical–extratropical teleconnection (across any critical latitudes). That is the main topic of this paper.

## 2. Observational aspects of intraseasonal oscillation

Several observational studies have contributed to our understanding of the Madden–Julian oscillation. Some of the observations that are important and relevant to this study are briefly reviewed in this section.

### 2.1. Global-scale phenomenon

Krishnamurti et al. (1990) has shown that this oscillation is a planetary-scale phenomenon. The 200-mb 30–50-day filtered divergent motion field has a distinct wave number zero signature with almost half the globe exhibiting a divergent outflow and the other half dominated by converging flows. In addition, Krishnamurti et al. (1992a) have examined the power spectra of the zonal wind in the wave number domain for the lower and the upper troposphere for the entire globe. It was shown that the major contribution to the total variance for the Madden–Julian time scale comes from the first six or seven zonal harmonics with the largest contribution coming from the planetary scales, substantiating the global-scale nature of the intraseasonal oscillation.

Fig. 2 (Krishnamurti and Gadgil, 1985) illustrates the global variation of the intraseasonal oscillation of the zonal wind at 850 mb for the four seasons. In Fig.

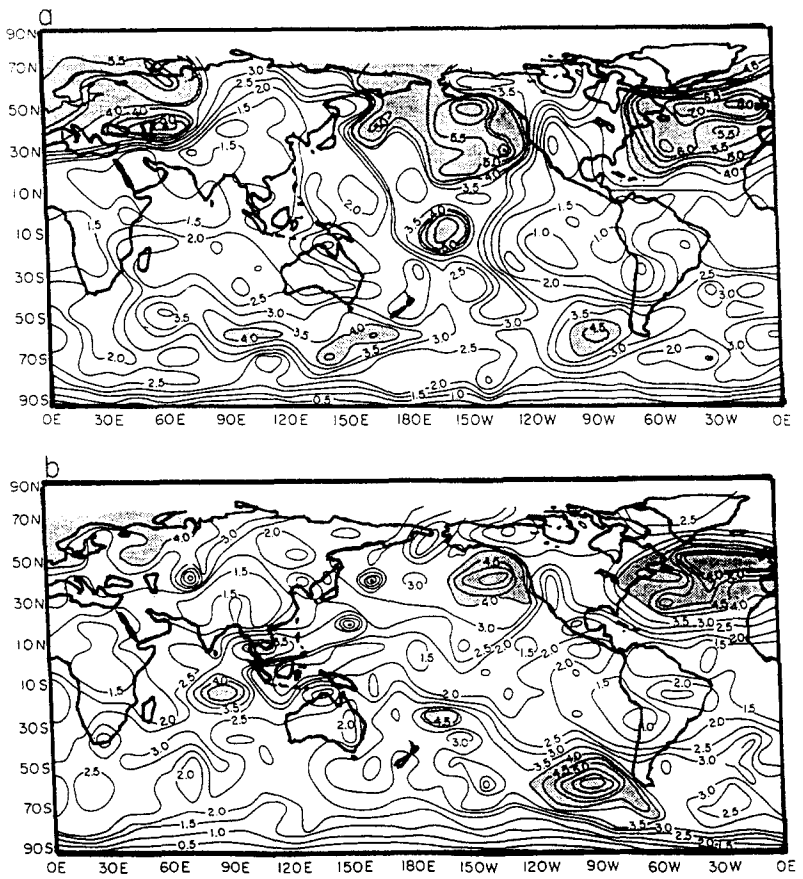


Fig. 2. The maximum seasonal amplitude of the intraseasonal oscillation of the zonal wind (m $s^{-1}$) for the FGGE year 1978–1979. (a) December, January, February; (b) March, April, May; (c) June, July, August; (d) September, October, November. These are based on Krishnamurti and Gadgil (1985).

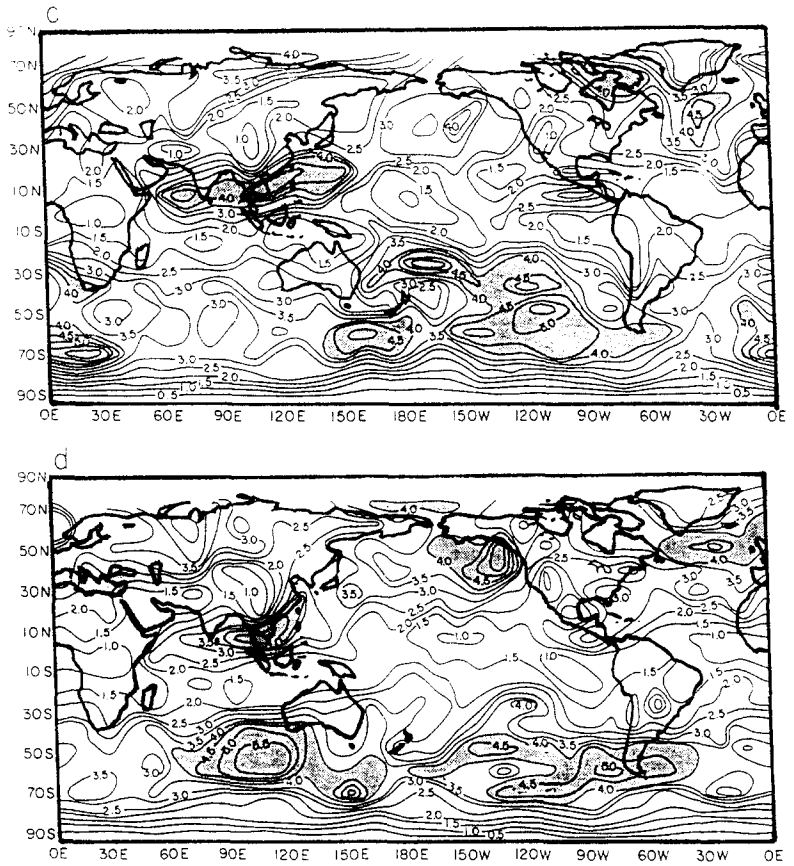


Fig. 2 (continued).

2(a)–(d), the winter season extends from December 1, 1978 through February 28, 1979, the spring season from March 1, 1979 through May 31, 1979, summer from June 1, 1979 through August 31, 1979 and autumn goes from September 1, 1979 through November 30, 1979. It is evident from the figures that in all four seasons the amplitude of the zonal wind oscillation is large at higher latitudes as compared with the lower latitudes. Furthermore, the winter hemisphere exhibits larger amplitudes compared with the summer hemisphere. Despite these large amplitudes in the extratropics, it was noted (Krishnamurti et al., 1992a) that the percent variance of the oscillation was smaller for the extratropics compared with the tropics. This is related to the stronger high-frequency variability over the extratropics. As the Northern Hemisphere summer approaches, large amplitudes of low-frequency components develop over the Asian monsoon region extending from Bay of Bengal to W. Pacific through southern Indo-China. In the spring months, the entire belt of the southwest monsoon from the Arabian Sea to West Pacific in summer exhibits a large monsoonal wind maxima. Krishnamurti et al. (1992a) noted that 20–25% of the total variance of the 850-mb variability was explained by the low-frequency component in the tropics.

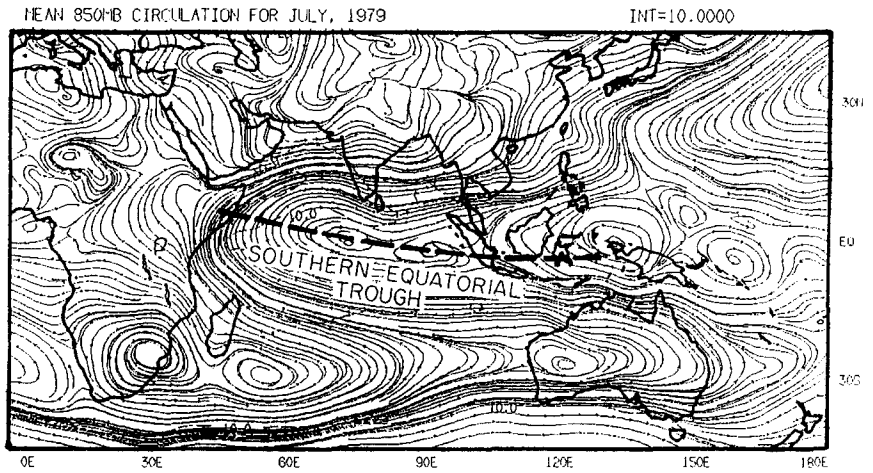


Fig. 3. Mean 850-mb flow field for July 1979. The southern equatorial trough is emphasized by a heavy dashed line. These are based on Krishnamurti et al. (1990).

## 2.2. *Source of the intraseasonal oscillation*

The origin of the meridionally propagating intraseasonal oscillations has been traced to the convectively active regions along the equatorial latitudes. Comeaux (1991), using the 1979 Monsoon Experiment (MONEX) data sets, noted that the eastward-propagating planetary-scale waves on the time scale of 30–50 days initiated the meridionally propagating waves as they passed over the longitudes of the southern equatorial trough (Fig. 3). In this illustration we show the climatological analysis of the motion field at the 850-mb level. The emphasis here is on the southern equatorial trough, whose axis is located roughly along the equator.

This is also evident in the latitude–time cross-section of the 30–50-day filtered outgoing long-wave radiation (OLR) and precipitation averaged between 70°E and 85°E for the Northern Hemisphere summer months of 1979 (Fig. 4(a) and (b)). These figures show clearly the meridional passage of waves in the OLR and the precipitation fields. They seem to originate from around 5°S which is the climatological location of the southern equatorial trough. Krishnamurti and Gadgil (1985) presented pressure–time cross-sections of the intraseasonal oscillation of the zonal wind over several selected points in the tropics (Arabian Sea and Caribbean) and mid-latitudes (over Northern Atlantic and Pacific Oceans); they noted a baroclinic vertical structure (Fig. 5(a) and (b)) with a phase reversal with altitude for the intraseasonal component over the tropics whereas in the mid-latitudes a more barotropic vertical structure (Fig. 5(c) and (d)) was noted. A strong upward propagation noted in the tropical latitudes (Krishnamurti and Gadgil, 1985) suggests a convective origin for this oscillation. Furthermore it is seen from Fig. 5(c) and (d) that the amplitude of this oscillation increases with altitude. Krishnamurti and Gadgil (1985) attribute this feature to the non-linear energy exchange between the barotropic transients and the strong zonal flow which increases with height.

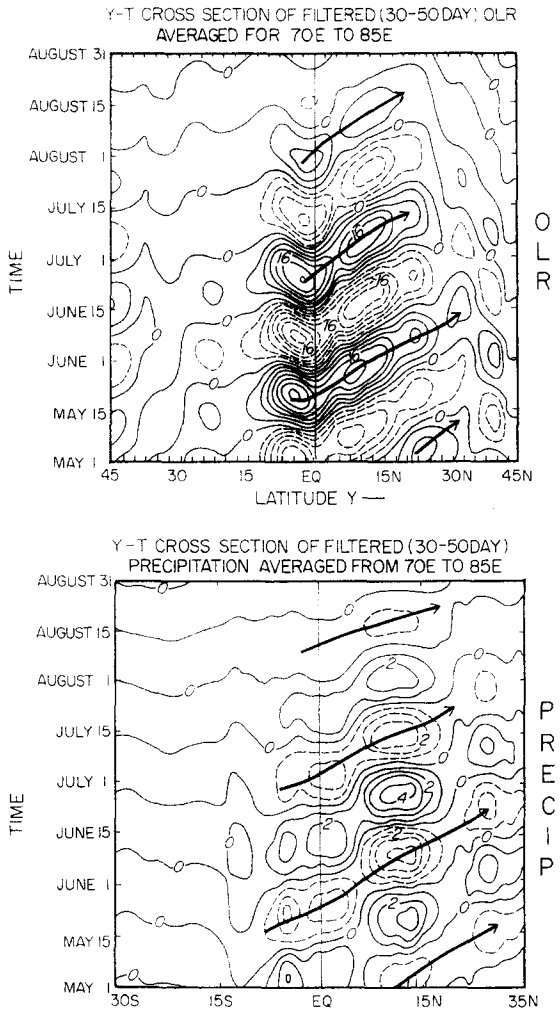


Fig. 4. Latitude–time plots of the anomalies of (a) the outgoing long-wave radiation (W $m^{-2}$) and (b) precipitation (mm $day^{-1}$). These anomalies are on the time scale of 30–50 days. The arrows denote meridional wave propagations.

### 2.3. Intraseasonal oscillation in monsoons

Several studies have indicated the modulation of the monsoons (Indian, Chinese and Australian) with the meridional passage of the intraseasonal oscillations on the time scale of 30–50 days. There are two important time scales in the context of these dry and wet spells. One of these is the time-averaged seasonal mean flow field which describes the climatology. The other time scale is the intraseasonal component which exhibits a meridional passage. During its passage, the intraseasonal wave can be in or out of phase with respect to the climatological component. This leads to parallel and antiparallel geometry for these two time scales.

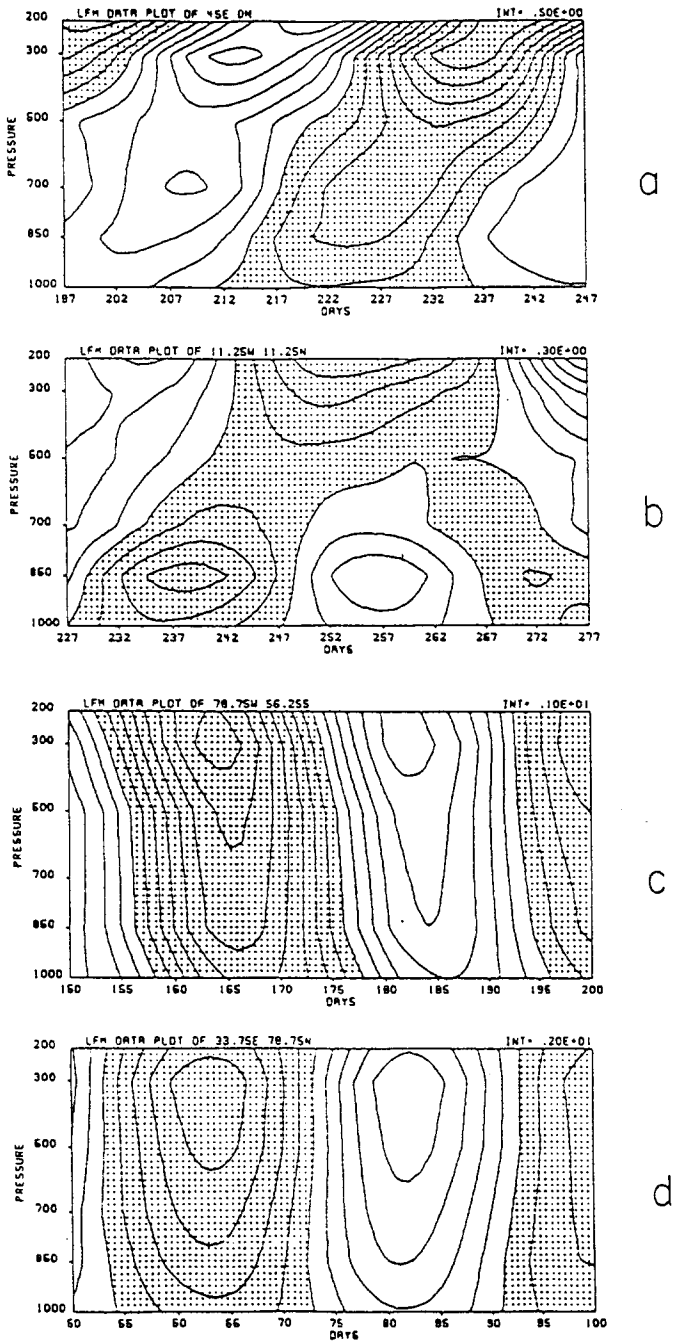


Fig. 5. Pressure–time sections of the intraseasonal component of the zonal wind at (a) 45°E, 0°N; (b) 11.25°W, 11.25°N; (c) 78.25°W, 56.25°S; (d) 33.75°E, 75.75°N. These are based on Krishnamurti and Gadgil (1985).

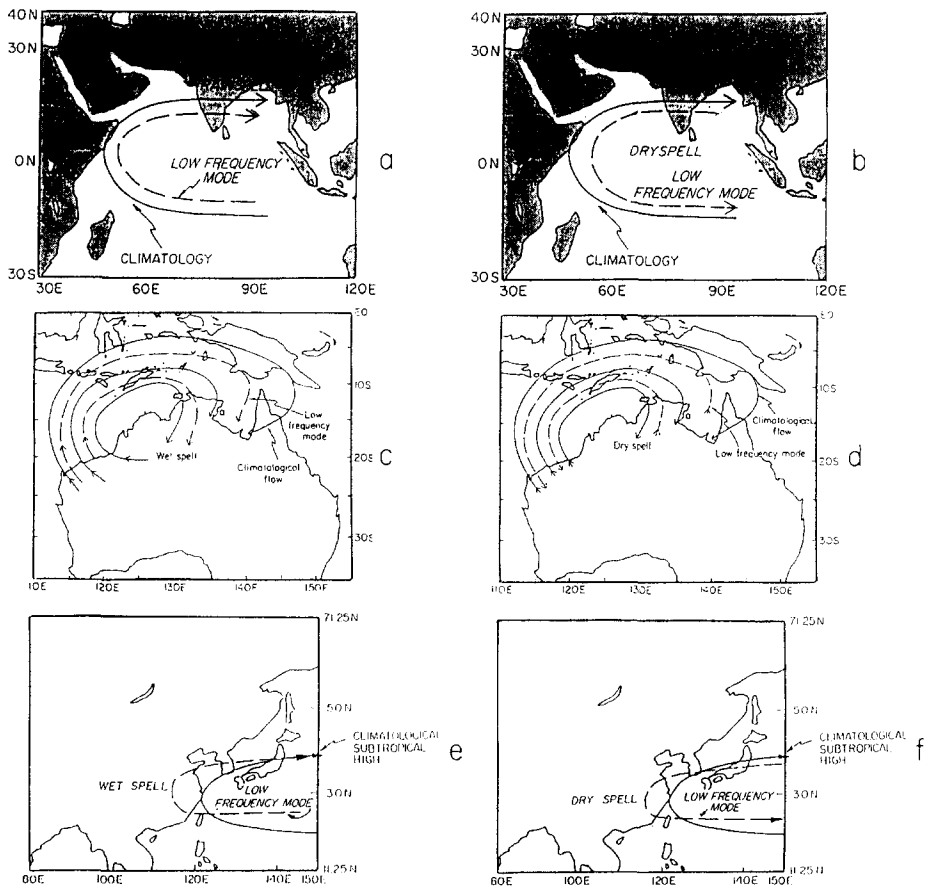


Fig. 6. Schematic plots of the parallel and antiparallel flows among the intraseasonal and the climatological components. (a) Indian monsoon wet spell (based on Krishnamurti et al., 1992a); (b) Indian monsoon dry spell (based on Krishnamurti et al., 1992a); (c) Australian monsoon wet spell (based on Krishnamurti et al., 1995); (d) Australian monsoon dry spell (based on Krishnamurti et al., 1995); (e) Chinese monsoon wet spell (based on Krishnamurti et al., 1992a); (f) Chinese monsoon dry spell (based on Krishnamurti et al., 1992a).

Typical anti-parallel flow regimes of the low-frequency motion relative to the climatological flows are illustrated in Fig. 6(b), (d) and (f) over Indian, Australian and Chinese regions, which entail a dry spell of the monsoon. Similarly parallel flow patterns such as shown in Fig. 6(a), (c) and (e) could favor a wet spell of the monsoon.

Fig. 7, based on Krishnamurti et al. (1990) shows a sequence of parallel and anti-parallel flow regimes at 850 mb over India using the First GARP Global Experiment (FGGE) data for the period July 31 to September 4, 1979. The panels of maps are shown at intervals of 5 days. Here the streamlines and isotachs (m $s^{-1}$) of the 850-mb flows on the time scale of 30–50 days are illustrated. The heavy solid line illustrates a clockwise gyre which denotes anticyclonic flows over the Northern Hemisphere. This gyre comes in and out of phase with respect to the climatological flows contributing to

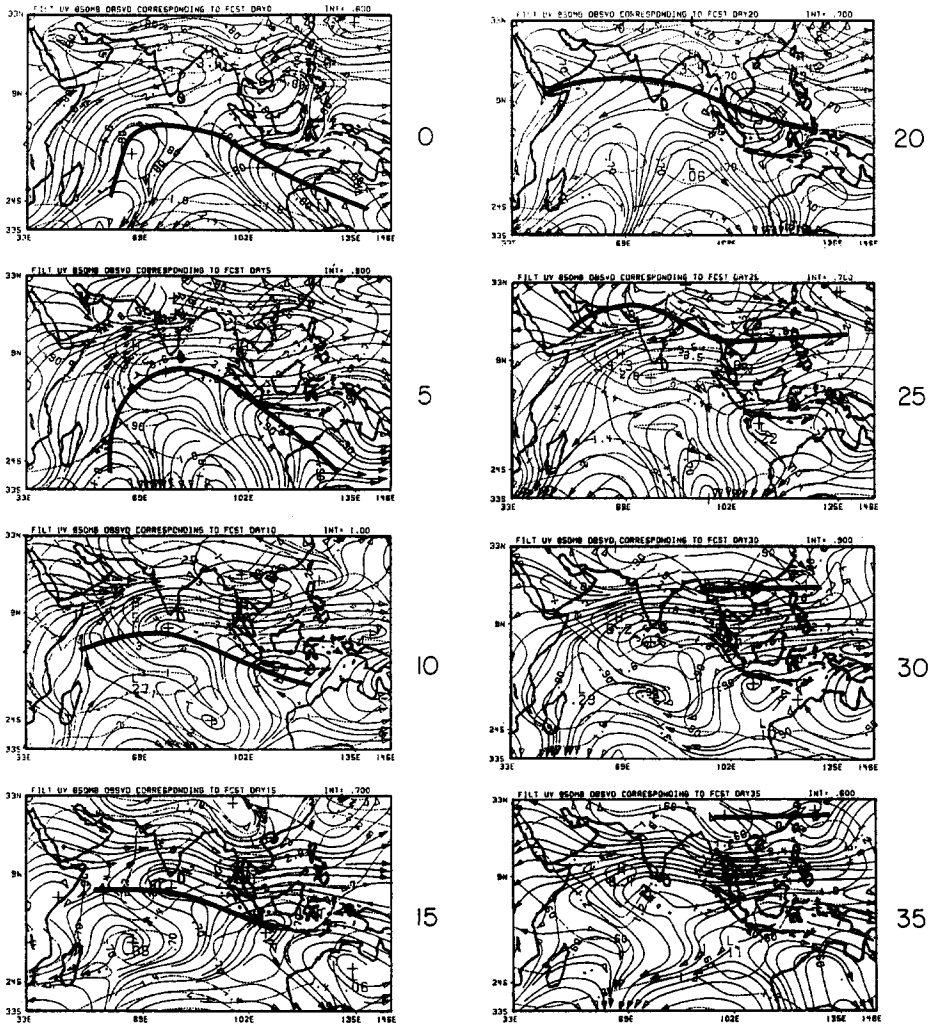


Fig. 7. Thirty-to-50-day time filtered flow field at 850 mb from July 31 through September 4, 1979 (at intervals of 5 days), based on observations (streamlines, solid lines; isotachs, dashed lines (m $s^{-1}$)). These are based on Krishnamurti et al. (1990).

enhance on-shore (wet spell) and off-shore (dry spell) flows. A similar depiction of the low-frequency flows over China (and east Asia) is shown in Fig. 8. Here we see the meridional passage of clockwise gyres that enhance (or weaken) the flows of the climatological subtropical high of the western Pacific Ocean. Here again the on-shore and off-shore flows, respectively, coincide with wet and dry spells of the Chinese monsoon. A typical sequence of the meridional passage of a rainfall event over China is illustrated in Fig. 9. This is based on Krishnamurti et al. (1992a). Here the 24-hourly rainfall at raingauge sites over China is shown at intervals of roughly 5 days. The shaded areas denote heavy rains. The heavy rainfall over the southeast coast of China (June 8,

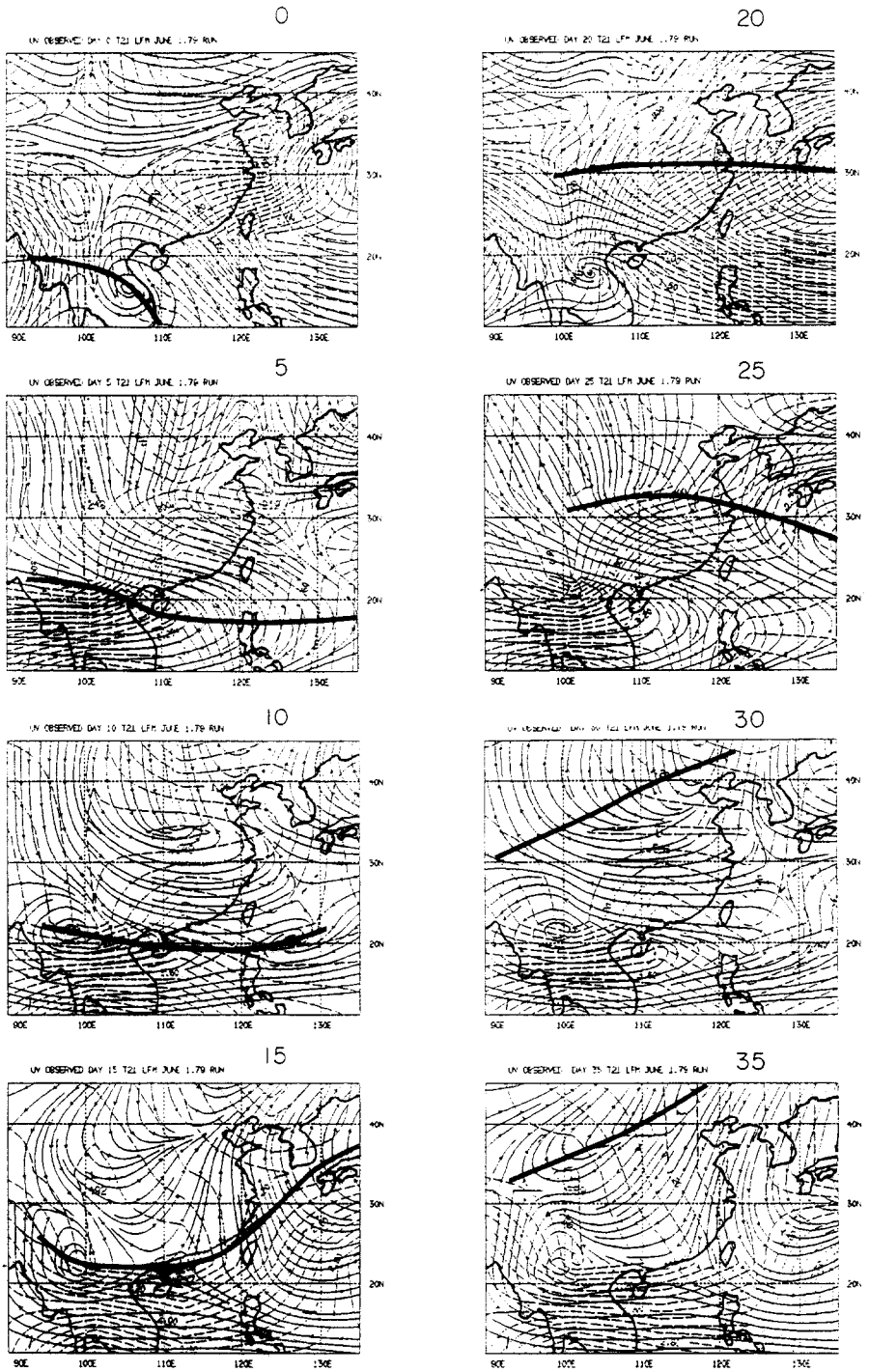


Fig. 8. Panels of the observed wind field (streamlines, solid lines; isotachs, dashed lines ($m\ s^{-1}$)). Day 0 is 1 June 1979. Maps shown at interval of 5 days. These are based on Krishnamurti et al. (1992a).

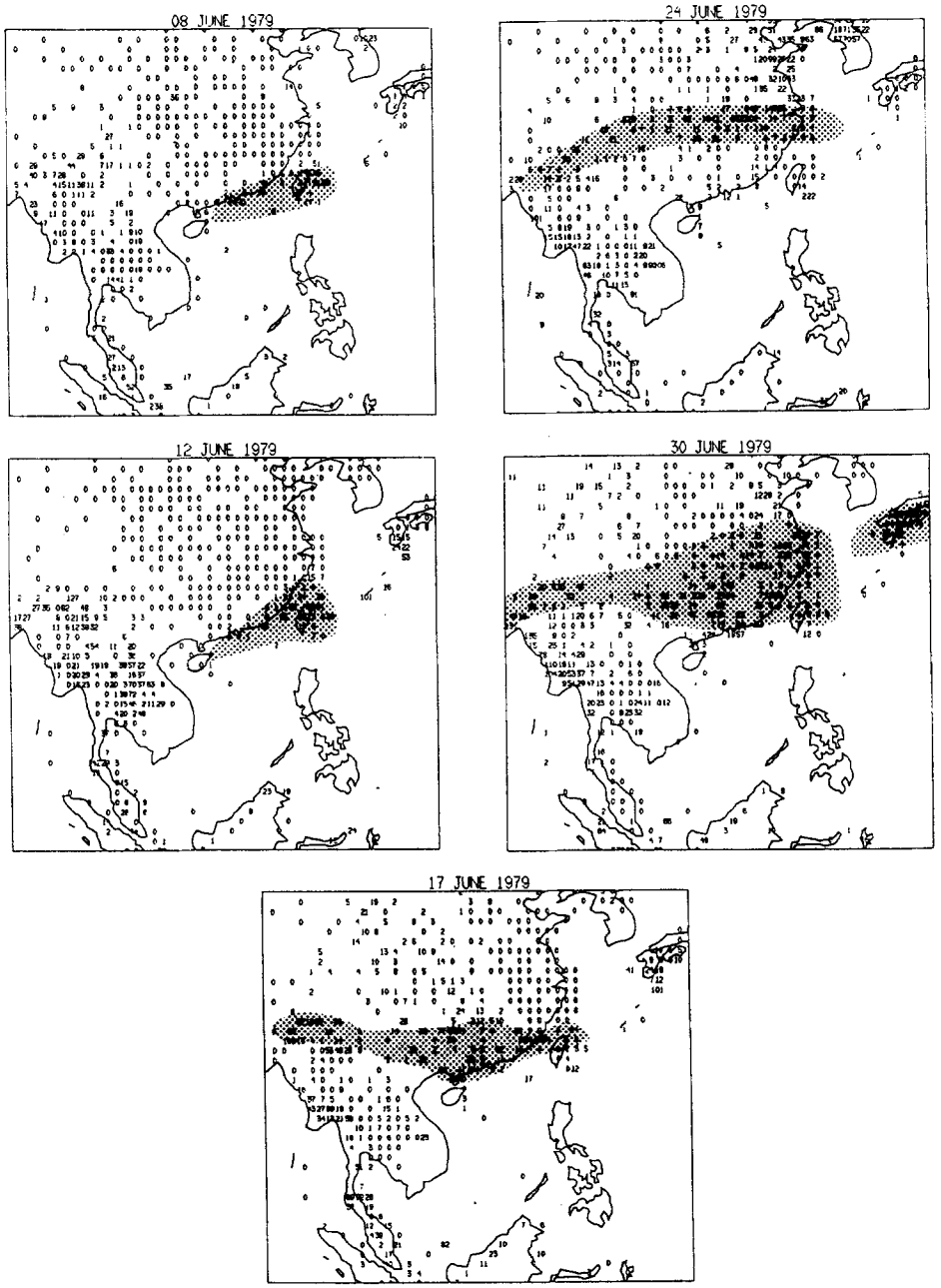


Fig. 9. A time sequence of observed 24-h rainfall totals (mm day$^{-1}$) on ten latitude–longitude squares over China based on raingauge data from the FGGE IIc archives: 8, 12, 17, 24 and 30 June 1979. These are based on Krishnamurti et al. (1992a).

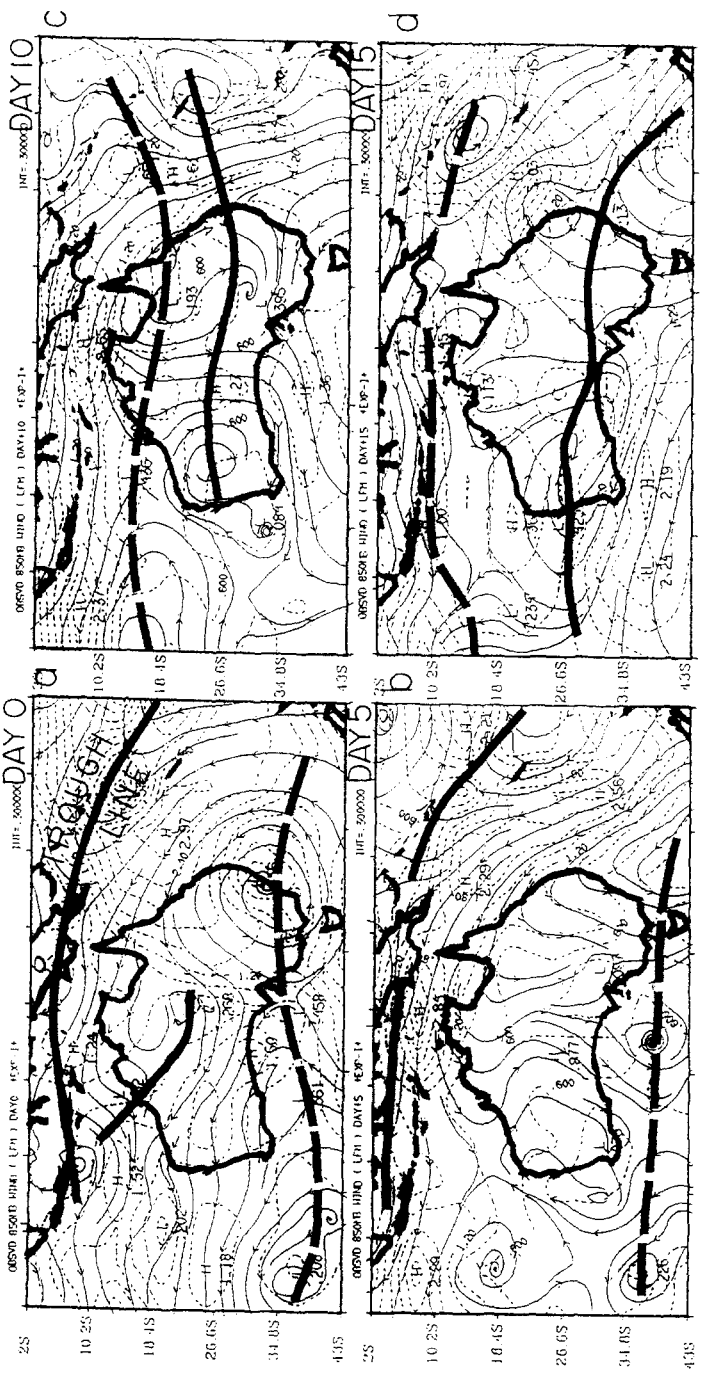


Fig. 10. Observed 30–60-day time-filtered flow field at 850 hPa from March 1 to March 30, 1992 at intervals of 5 days. Streamlines (solid lines) and isotachs (dashed lines) at intervals of 0.3 m $s^{-1}$. Thick lines are trough lines and thick dashed lines are ridge lines. These are based on Krishnamurti et al. (1995).

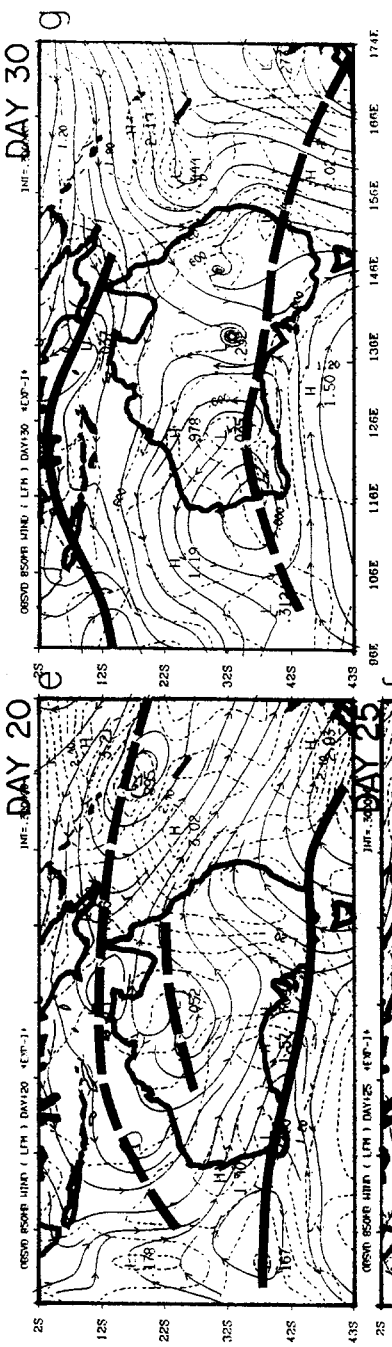


Fig. 10 (continued).

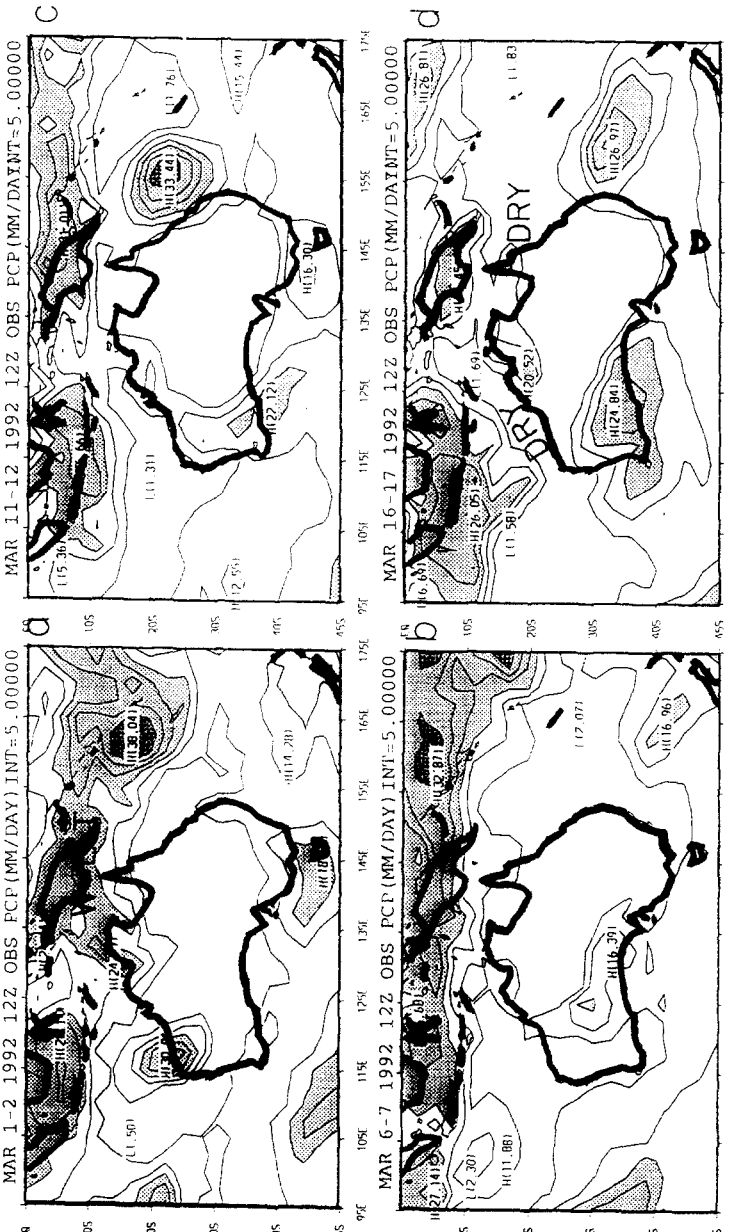


Fig. 11. Observed 24-h rainfall totals (mm day$^{-1}$) through the month of March 1992, at intervals of 5 days. Intervals of isopleths are 5.00 mm day$^{-1}$. These are based on Krishnamurti et al. (1995).

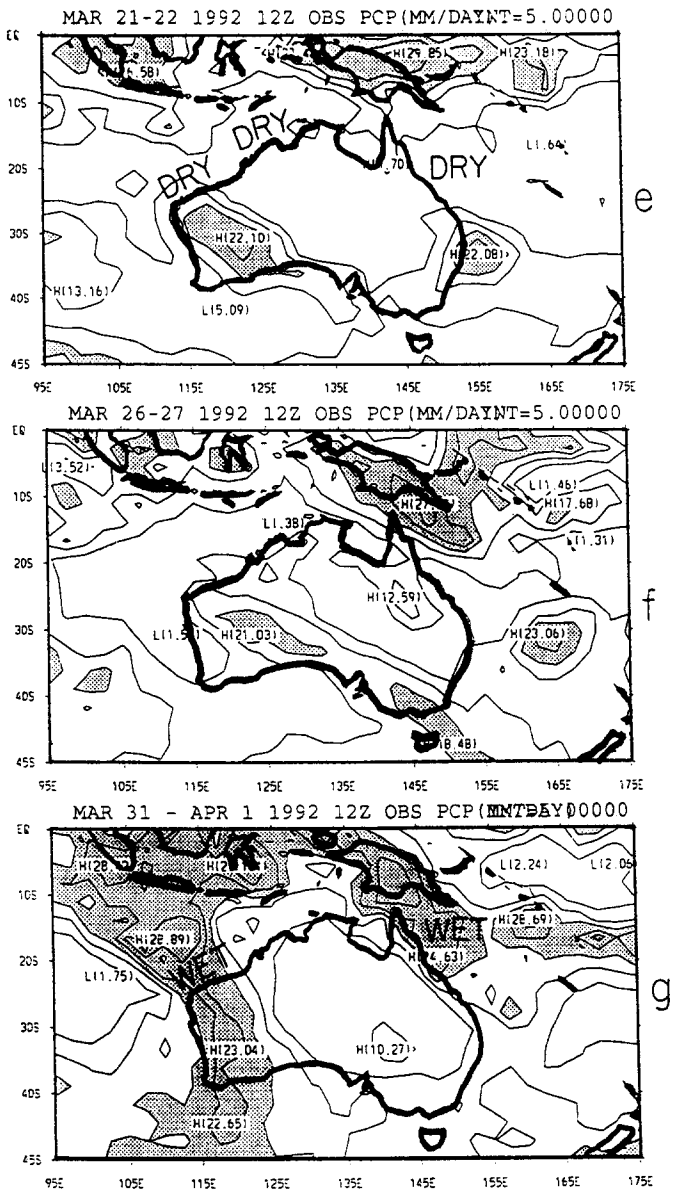


Fig. 11 (continued).

1979) exhibits a slow northward motion with time, and it arrives over central China by the 30 June. This enhancement of rain over central China occurred as the low-frequency component came in phase with the on-shore flows of the climatological subtropical high, thus enhancing the moisture supply over land. The passage of a low-frequency cyclonic

component of the flow field across the northern part of Australia is known to coincide with the active spells of the Australian monsoon (Hendon and Liebmann, 1990; Krishnamurti et al., 1995). This is illustrated in Fig. 10(a)–(g) (Krishnamurti et al., 1995). These are a sequence of 850-mb flow fields on the time scale of 30–50 days. Here we have emphasized the trough line by a heavy solid line and the ridge line by a dashed line. These illustrations cover the period March 1 to March 30, 1992; and maps are shown at intervals of 5 days. Cyclonic troughs of the low-frequency motion were located over northern Australia in the beginning and end of the month, whereas a ridge line was present over the region around the 15 March. These lines exhibited a poleward (southward) motion during this month. Rainfall distribution (Fig. 11(a)–(g); Krishnamurti et al., 1995) exhibited wet spells of the Australian monsoon during the beginning and end of the month. A dry spell prevailed over northern Australia during the middle of

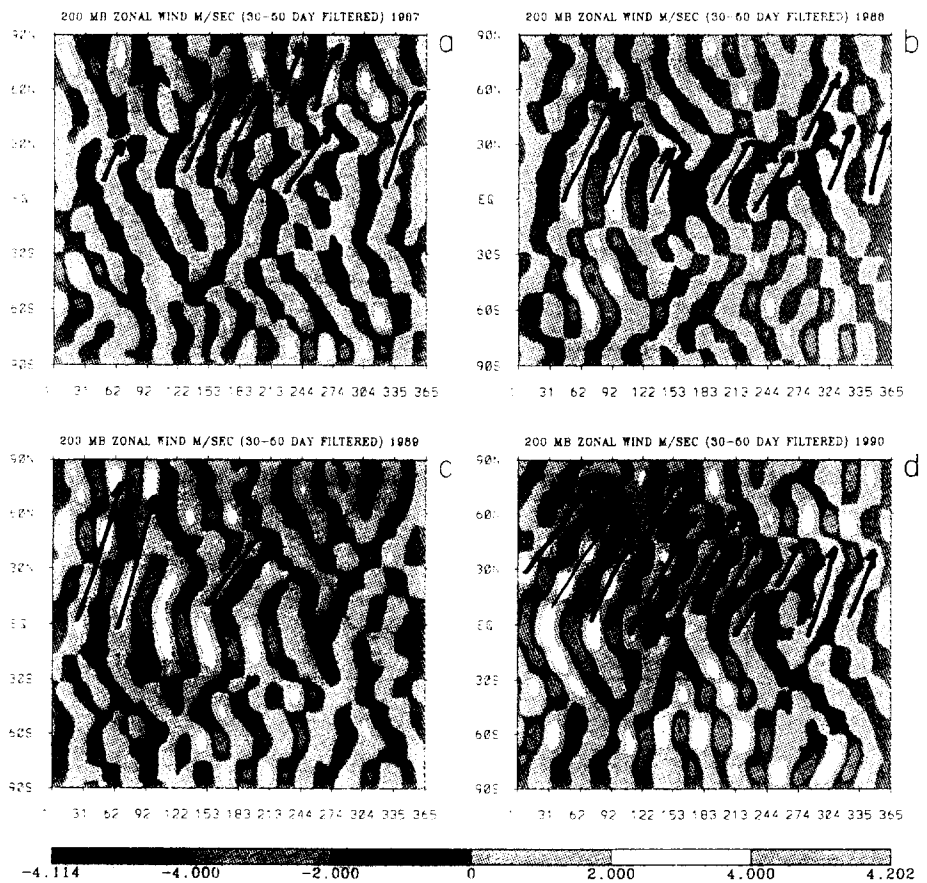


Fig. 12. Latitude–time diagram of the zonally averaged zonal-flow anomalies on the time scale of 30–50 days. The eight panels show the results at 200 mb for the years 1987 through 1994. The heavy arrows denote a poleward propagation of the zonal flow anomalies. units, m $s^{-1}$; intervals, 1 m $s^{-1}$.

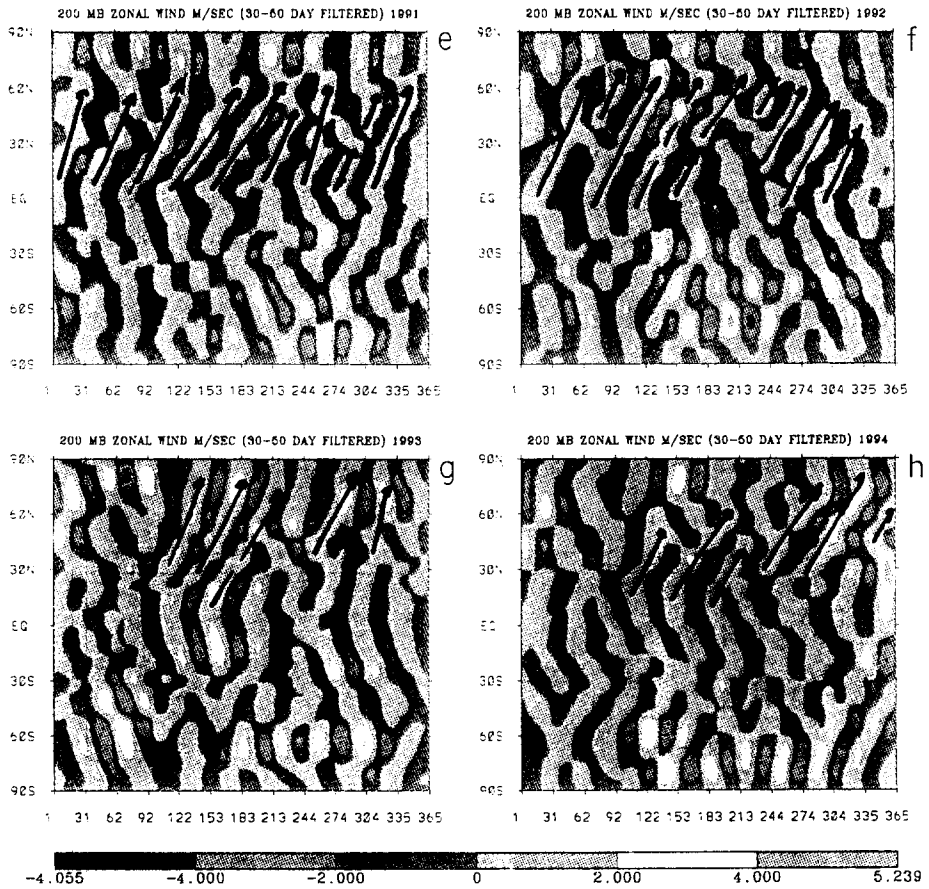


Fig. 12 (continued).

the month. These are the daily observed rainfall totals based on surface and satellite based measurements (Goirala and Krishnamurti, 1992).

## 3. Data sets

The data sets used for this research work were obtained from the ECMWF analyses for the years 1987–1994. These contain the daily fields at ten pressure levels: 1000 hPa, 850 hPa, 700 hPa, 600 hPa, 500 hPa, 400 hPa, 300 hPa, 250 hPa, 200 hPa and 100 hPa. The horizontal resolution of the data set is 2.5° lat./long. The relevant variables for this study included the winds, temperature and the geopotential.

## 4. Linear theory

The expression for meridional wave energy flux following the linear theory can be obtained from the equations of motion, mass continuity and the thermodynamic equa-

tion. Essentially this is the meridional analog of the Eliassen and Palm (1961) work on the vertical wave energy flux problem. Thus following Yanai and Lu (1983), we have,

$$\overline{\phi' v'} = -(\bar{u} - c)\left[\overline{u' v'} - \frac{1}{\sigma_0}\frac{\overline{\partial u}}{\partial p}\frac{\overline{v' \partial \phi'}}{\partial p}\right] \tag{1}$$

Here $\overline{\phi' v'}$ denotes the wave energy flux across a latitude circle; $\bar{u}$ is the zonally averaged zonal wind; $c$ is the phase speed of the wave; $\overline{u' v'}$ denotes the meridional eddy flux of momentum; $\sigma_0$ is a reference dry static stability; $\partial \bar{u}/\partial p$ denotes the vertical shear of the zonally averaged zonal wind; $v' \dfrac{\overline{\partial \phi}}{\partial p}$ is a measure of the meridional heat flux across a latitude circle.

It should be noted that the wave energy flux vanishes where $\bar{u} - c$ vanishes. That latitude is usually designated as the critical latitude. Furthermore, Krishnamurti et al. (1992b) have shown the zonally averaged zonal flows exhibit a large intraseasonal

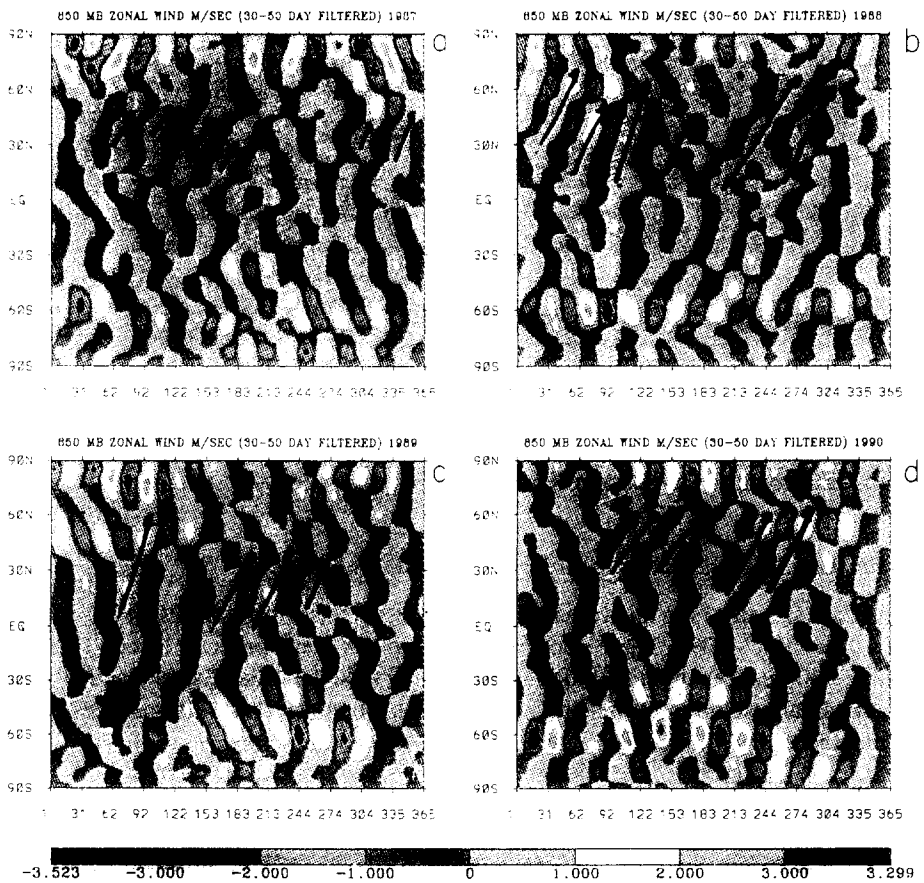


Fig. 13. Same as Fig. 12, but at the 850-mb surface.

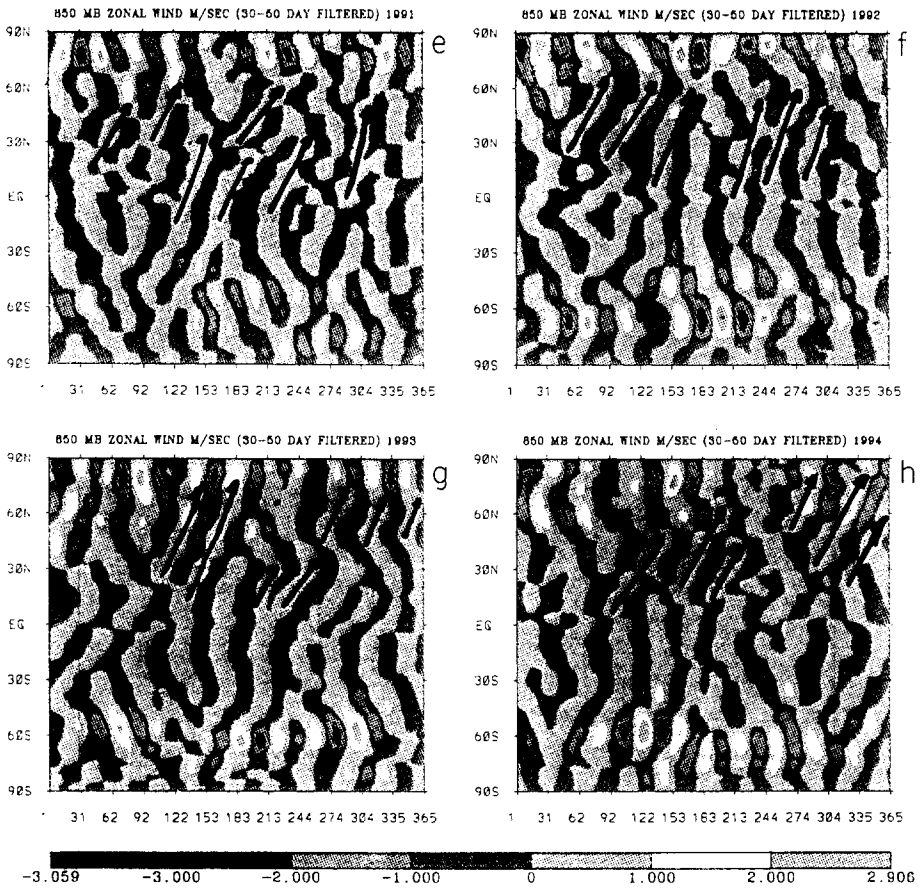


Fig. 13 (continued).

variability. Thus the assumption of a time-invariant zonal flow for the studies of wave energy fluxes in the intraseasonal time scales appears invalid. The linear theory sees time-invariant easterlies of the tropical latitudes separated from the westerlies of the higher latitudes. A critical latitude exists close to this latitude separating the easterlies from westerlies where the parameter $(\bar{u} - c)$ vanishes. It is apparent that we need to examine this problem in a non-linear context where the wave energy fluxes include the zonal-flow variations on the intraseasonal time scales.

Fig. 12 and Fig. 13 illustrate the latitude–time (daily) variations of the zonal flows on the time scale of the intraseasonal oscillation for 200 and 850 hPa. In these illustrations, aside from the alteration in sign, we note clear signals of meridional (poleward) propagation of the zonal-flow anomalies on this time scale. The maximum amplitudes of these zonal-flow oscillations are of the order of 1–3 m $s^{-1}$. Furthermore upon closer inspection, we find an essential barotropic character in the data at these two levels, i.e. meridionally propagating zonal-flow anomalies at the two levels appear to overlay each other.

We shall next examine the non-linear problem of the wave energy flux where we invoke variations in zonal flows in order to examine their intraseasonal contributions.(Figs. 13 and 14)

## 5. Non-linear wave energy flux

In this section we shall first derive an expression for the wave energy flux using the equations of motion, the first law of thermodynamics and the mass conservation law.

The zonal equation of motion:

$$\frac{\partial u}{\partial t} + \frac{1}{R\cos\theta}\frac{\partial}{\partial\lambda}(u^2) + \frac{1}{R\cos^2\theta}\frac{\partial}{\partial\theta}(vu\cos^2\theta) + \frac{\partial}{\partial p}(\omega u) - fv + \frac{1}{R\cos\theta}\frac{\partial\phi}{\partial\lambda} = 0 \tag{2}$$

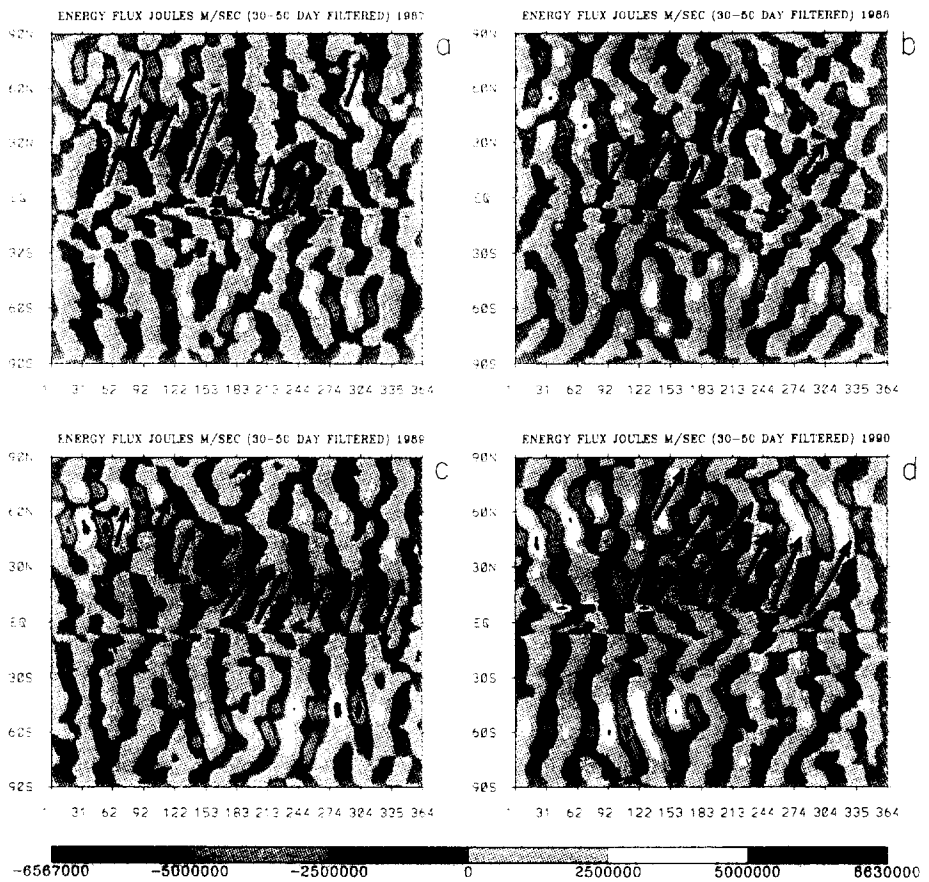


Fig. 14. Latitude–time diagram of meridional wave energy flux $\overline{\phi' v'}$ on the time scale of 30–50 days. Eight separate years of results are shown for the years 1987 through 1994 here. The ordinate denotes latitude, the abscissa denotes day of the year. Units are J m $s^{-1}$. The heavy arrows denote channels of strong meridional poleward flows.

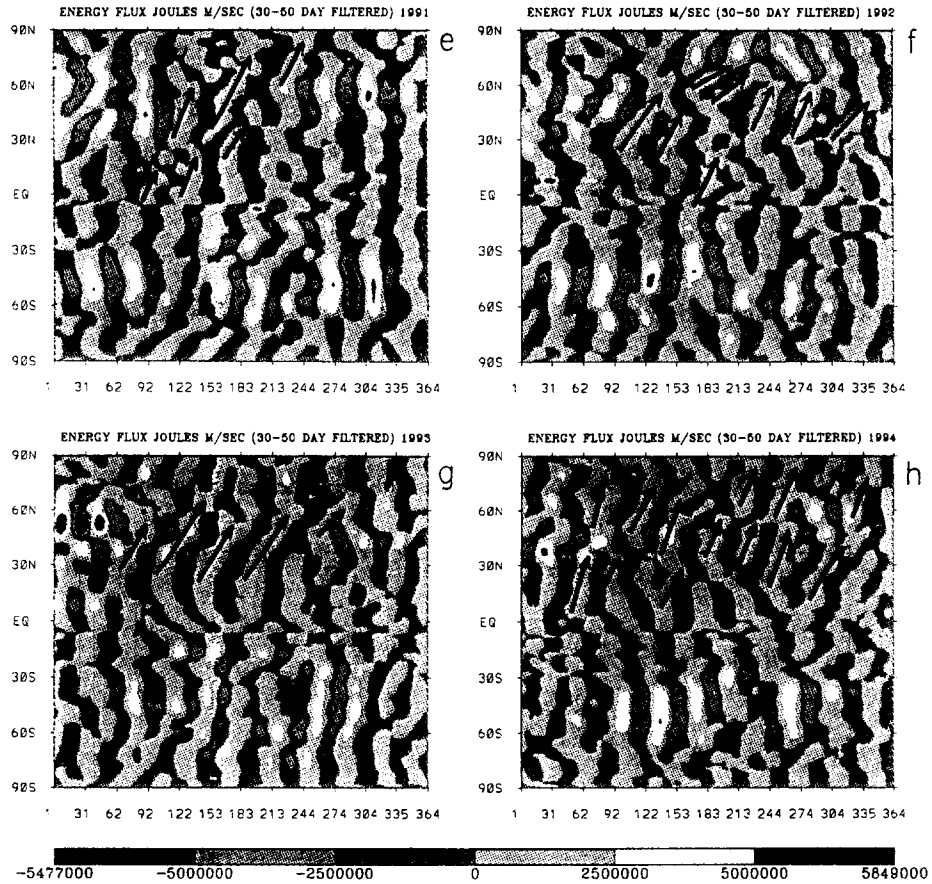


Fig. 14 (continued).

The meridional equation of motion:

$$\frac{\partial v}{\partial t} + \frac{1}{R\cos\theta}\frac{\partial}{\partial\lambda}(uv) + \frac{1}{R\cos\theta}\frac{\partial}{\partial\theta}(v^2\cos\theta) + \frac{\partial}{\partial p}(\omega v) + fu + \frac{u^2\tan\theta}{R} + \frac{1}{R}\frac{\partial\phi}{\partial\theta} = 0 \tag{3}$$

The adiabatic law:

$$\frac{\partial}{\partial t}\left(\frac{\partial\phi}{\partial p}\right) + \frac{u}{R\cos\theta}\frac{\partial}{\partial\lambda}\left(\frac{\partial\phi}{\partial p}\right) + \frac{v}{R}\frac{\partial}{\partial\theta}\left(\frac{\partial\phi}{\partial p}\right) + \sigma_0\omega = 0 \tag{4}$$

The mass continuity equation:

$$\frac{1}{R\cos\theta}\frac{\partial u}{\partial\lambda} + \frac{1}{R\cos\theta}\frac{\partial(v\cos\theta)}{\partial\theta} + \frac{\partial\omega}{\partial p} = 0 \tag{5}$$

We shall next perform a perturbation analysis with respect to the zonal mean (defined with an overbar) using the relations:

$$u = \bar{u} + u',\ v = v',\ \omega = \omega',\ \phi = \bar{\Phi} + \phi',\ \bar{u} = \bar{u}(\theta, p),\ \bar{\phi} = \bar{\phi}(\theta, p) \tag{6}$$

Here $\bar{u}$ is the zonal mean flow and $\bar{\Phi}$ is defined from a geostrophic relation, which is the mean meridional equation of motion in the form:

$$f\bar{u} + \frac{\bar{u}^2 \tan\theta}{R} + \frac{1}{R}\frac{\partial \bar{\Phi}}{\partial \theta} = 0 \tag{7}$$

Upon differentiating with respect to pressure we obtain the thermal wind relation:

$$\left(2\bar{u}\frac{\tan\theta}{R} + f\right)\frac{\partial \bar{u}}{\partial p} = -\frac{1}{R}\frac{\partial}{\partial \theta}\left(\frac{\partial \bar{\phi}}{\partial p}\right) \tag{8}$$

Upon subtracting the mean flow equations (Eqs. (6)–(8)) from the equations of total flow (Eqs. (2)–(5)) we obtain the following equations for the perturbations:

$$\frac{\partial u'}{\partial t} + \frac{2\bar{u}}{R\cos\theta}\frac{\partial u'}{\partial \lambda} + \frac{1}{R\cos^2\theta}\frac{\partial}{\partial \theta}(\bar{u}v'\cos^2\theta) + \frac{\partial}{\partial p}(\bar{u}\omega') - fv' + \frac{1}{R\cos\theta}\frac{\partial \phi'}{\partial \lambda}$$
$$= -\left[\frac{1}{R\cos\theta}\frac{\partial}{\partial \lambda}(u'^2) + \frac{1}{R\cos^2\theta}\frac{\partial}{\partial \theta}(v'u'\cos^2\theta) + \frac{\partial}{\partial p}(\omega'u')\right] \tag{9}$$

$$\frac{\partial v'}{\partial t} + \frac{1}{R\cos\theta}\frac{\partial}{\partial \lambda}(\bar{u}v') + \frac{2\bar{u}u'\tan\theta}{R} + fu' + \frac{1}{R}\frac{\partial \phi'}{\partial \theta}$$
$$= -\left[\frac{1}{R\cos\theta}\frac{\partial}{\partial \theta}(v'^2\cos\theta) + \frac{1}{R\cos\theta}\frac{\partial}{\partial \lambda}(v'u') + \frac{\partial}{\partial p}(\omega'v') + \frac{u'2\tan\theta}{R}\right] \tag{10}$$

$$\frac{\partial}{\partial t}\left(\frac{\partial \phi'}{\partial p}\right) + \frac{\bar{u}}{R\cos\theta}\frac{\partial}{\partial \lambda}\left(\frac{\partial \phi'}{\partial p}\right) + \frac{v'}{R}\frac{\partial}{\partial \theta}\left(\frac{\partial \bar{\Phi}}{\partial p}\right) + \sigma_0\omega'$$
$$= -\left[\frac{u'}{R\cos\theta}\frac{\partial}{\partial \lambda}\left(\frac{\partial \phi'}{\partial p}\right) + \frac{v'}{R}\frac{\partial}{\partial \theta}\left(\frac{\partial \phi'}{\partial p}\right)\right] \tag{11}$$

$$\frac{1}{R\cos\theta}\frac{\partial u'}{\partial \lambda} + \frac{1}{R\cos\theta}\frac{\partial}{\partial \theta}(v'\cos\theta) + \frac{\partial \omega'}{\partial p} = 0 \tag{12}$$

On substituting for $\frac{1}{R}\frac{\partial}{\partial \theta}\left(\frac{\partial \bar{\phi}}{\partial p}\right)$ from (8) into (11), we can write the equations (9) through (11) as follows:

$$\frac{\partial u'}{\partial t} + \frac{1}{R\cos\theta}\frac{\partial}{\partial \lambda}\left[2\bar{u}u' + u'^2 + \phi'\right] + \frac{1}{R\cos^2\theta}\frac{\partial}{\partial \theta}(\bar{u}v'\cos^2\theta) + \frac{\partial}{\partial p}(\bar{u}\omega') - fv'$$
$$= -\left[\frac{1}{R\cos^2\theta}\frac{\partial}{\partial \theta}(u'v'\cos^2\theta) + \frac{\partial}{\partial p}(\omega'u')\right] \tag{13}$$

$$\frac{\partial v'}{\partial t}+\frac{1}{R\cos\theta}\frac{\partial}{\partial\lambda}[\bar{u}v'+u'v']+\left(\frac{2\bar{u}\tan\theta}{R}+f\right)u'+\frac{1}{R}\frac{\partial\phi'}{\partial\theta}$$

$$=-\frac{1}{R\cos\theta}\frac{\partial}{\partial\theta}(v'^2\cos\theta)-\frac{\partial}{\partial p}(\omega'v') \tag{14}$$

$$\frac{\partial}{\partial t}\left(\frac{\partial\phi'}{\partial p}\right)+\frac{\bar{u}}{R\cos\theta}\frac{\partial}{\partial\lambda}\left(\frac{\partial\phi'}{\partial p}\right)-v'\left(\frac{2\bar{u}\tan\theta}{R}+f\right)\frac{\partial\bar{u}}{\partial p}+\sigma_0\omega'$$

$$=-\left[\frac{u'}{R\cos\theta}\frac{\partial}{\partial\lambda}\left(\frac{\partial\phi'}{\partial p}\right)+\frac{v'}{R\cos\theta}\frac{\partial}{\partial\theta}\left(\frac{\partial\phi'}{\partial p}\right)\right] \tag{15}$$

The derivation of the following expression for the total wave energy flux obtained on eliminating $\omega'$ from Eq. (13) using Eqs. (8), (12), (14) and (15) is presented in Appendix A.

$$\overline{\phi'v'}=\frac{1}{(f-\Gamma)}\left[\overline{\beta\phi'}+\overline{\left\{\frac{u'^2}{2}-\frac{1}{\sigma_0}\frac{\partial}{\partial p}\left(\frac{\bar{u}^2}{2}\right)\frac{\partial\phi'}{\partial p}\right\}\gamma}\right]$$

$$+\frac{1}{(f-\Gamma)}\left(\overline{\phi'\gamma}+\bar{u}(\overline{\beta u'}+\overline{\gamma u'})\right)-\overline{\frac{1}{\sigma_0}\frac{1}{(f-\Gamma)}\frac{\partial u'}{\partial p}\frac{\bar{u}^2}{2}\left(\frac{\partial\phi'}{\partial p}\right)}$$

$$+\frac{1}{(f-\Gamma)}\overline{\left((\beta+\gamma)\left(\frac{u'^2}{2}-\frac{1}{\sigma_0}\frac{\partial}{\partial p}\left(\frac{\bar{u}^2}{2}\right)\frac{\partial\phi'}{\partial p}\right)\right)}$$

$$-\left(\overline{\bar{u}u'v'}+\overline{\left(\frac{u'^2}{2}-\frac{1}{\sigma_0}\frac{\partial}{\partial p}\left(\frac{\bar{u}^2}{2}\right)\frac{\partial\phi'}{\partial p}\right)v'}\right) \tag{16}$$

where

$$\beta=\frac{\partial}{\partial t}\left[u'-\frac{1}{\sigma_0}\frac{\partial\bar{u}}{\partial p}\frac{\partial\phi'}{\partial p}\right]-\frac{1}{\sigma_0}\frac{\partial}{\partial p}\left(\frac{u'^2}{2}\right)\cdot\frac{1}{R\cos\theta}\frac{\partial}{\partial\lambda}\left(\frac{\partial\phi'}{\partial p}\right)$$

$$\gamma=\left\{\frac{1}{R\cos\theta}\frac{\partial}{\partial\theta}(\bar{u}\cos\theta)+\frac{1}{\sigma_0}\frac{\partial\bar{u}}{\partial p}\left(\frac{2\bar{u}}{R}+f\right)\frac{\partial u'}{\partial p}-\frac{1}{\sigma_0}\frac{\partial\bar{u}}{\partial p}\frac{1}{R}\frac{\partial}{\partial\theta}\left(\frac{\partial\phi'}{\partial p}\right)\right.$$

$$\left.-\frac{1}{\sigma_0}\frac{\partial u'}{\partial p}\cdot\frac{1}{R}\frac{\partial}{\partial\theta}\left(\frac{\partial\phi'}{\partial p}\right)\right\}v'$$

and

$$\Gamma=\frac{1}{R}\frac{\partial\bar{u}}{\partial\theta}-\frac{\bar{u}\tan\theta}{R}-\frac{1}{R}\frac{\partial}{\partial\theta}\left(\frac{\partial\Phi}{\partial p}\right)\left(\frac{1}{\sigma_0}\frac{\partial\bar{u}}{\partial p}\right)$$

### 5.1. Computational procedure

In order to compute the total wave energy flux from Eq. (16), the following breakdown was made: $\overline{\phi' v'}$ = Linear variables + Quadratic terms + Triple product terms, where

$$\text{Linear variables} = \overline{\frac{1}{\sigma_0}\frac{1}{f-\Gamma}\frac{\partial u'}{\partial p}\frac{\partial}{\partial t}\left(\frac{\partial \phi'}{\partial p}\right)} + \overline{\left(\frac{u'^2}{2} - \frac{1}{\sigma_0}\frac{\partial}{\partial p}\left(\frac{\overline{u}^2}{2}\right)\frac{\partial \phi'}{\partial p}\right)v'} \tag{17a}$$

$$\text{Quadratic terms} = \left\{\frac{1}{f-\Gamma}\overline{\beta\phi'} + \frac{1}{f-\Gamma}\overline{\phi'\gamma}\right\} + \left(\frac{1}{f-\Gamma}\right)\overline{(\beta+\gamma)\left(\frac{u'^2}{2} - \frac{1}{\sigma_0}\frac{\partial}{\partial p}\left(\frac{\overline{u}^2}{2}\right)\frac{\partial \phi'}{\partial p}\right)} - (\overline{\overline{u}\overline{u'v'}}) \tag{17b}$$

$$\text{Triple product terms} = \frac{1}{f-\Gamma}\overline{\left(\frac{u'^2}{2} - \frac{1}{\sigma_0}\frac{\partial}{\partial p}\left(\frac{\overline{u}^2}{2}\right)\frac{\partial \phi'}{\partial p}\right)\gamma} + \frac{1}{f-\Gamma}\overline{u}\overline{\beta u'} + \frac{1}{f-\Gamma}(\overline{u\gamma u'}) \tag{17c}$$

Here the terms with overbars are zonal averages and are treated as single (time series) variables. All of these individual terms, for each member of the quadratic and triple product family, were calculated by finite differences at all vertical levels and at each location. These individual terms were pressure weighted and integrated for the entire vertical depth from 150 hPa to 925 hPa. Time series for each of these numbers of the quadratic and triple products were generated for each day for the 6 years of data.

Hayashi (1980) proposed that non-linear energy transfer spectra can be obtained simply by taking a Fourier transform of the product of the dependent variables which are multiplied at the grid points. This methodology, in principle, is similar to the method of computing a spherical harmonics transform of non-linear equations proposed by Orzag (1970) and by Eliasen et al. (1970). However, some information related to energy exchange among individual triad of components is lost from the latter approach.

Before proceeding to describe tide co-spectral method adopted to compute the non-linear terms, a few relevant definitions are presented. Any two-space and time-dependent variables $u$ and $v$ can be written as

$$u = u(\lambda, \phi, p, t) \quad \text{and} \quad v = v(\lambda, \phi, p, t)$$

These can next be represented by discrete Fourier transforms:

$$u_j = \sum_{n=0}^{N-1} U(n) e^{i2\pi nj/N} \tag{18a}$$

and

$$v_j = \sum_{n=0}^{N-1} V(n) e^{i2\pi nj/N} \tag{18b}$$

where $N$ is the total number of observations for the given time series. The sample co-spectral and quadrature spectra can then be defined from Jenkins and Watts (1968) as:

$$P_n(u,v) = \tfrac{1}{2}\mathrm{Re}(U_n^* V_n) \tag{19a}$$

$$Q_n(u,v) = \tfrac{1}{2}\mathrm{Im}(U_n^* V_n) \tag{19b}$$

Where $^*$ represent complex conjugates and $U_n$ and $V_n$ are Fourier coefficients. The sample co-spectrum is interpreted as the spectrum of sample covariance averaged over time. The sample quadratic spectrum is interpreted as the out-of-phase co-spectrum between $u$ and $v$ (90° phase shift)

$$Q_n(u,v) = \frac{N\Delta t}{2n\pi} P_n\left(u, \frac{\partial v}{\partial t}\right) \tag{20}$$

More generally, the sample cross-spectra $R_n(u, v)$ are defined as

$$R_n(u,v) = P_n(u,v) + iQ_n(u,v) \tag{21}$$

Therefore the frequency co-spectra of the quadratic terms in equation Eq. (17a) can be written as:

$$P_n\left(\frac{1}{f-\Gamma}, \overline{\beta\phi'}\right) + P_n\left(\frac{1}{f-\Gamma}, \overline{\phi' v}\right) + P_n\left(\frac{1}{f-\Gamma}, \overline{(\beta+\gamma)\left(\frac{u'^2}{2} - \frac{1}{\sigma_0}\frac{\partial}{\partial p}\left(\frac{\bar{u}^2}{2}\right)\frac{\partial\phi'}{\partial p}\right)}\right) - P_n\left(\bar{u}, \overline{u'v'}\right) \tag{22a}$$

While the frequency co-spectra of triple products in Eq. (17b) is expressed by:

$$P_n\left(\frac{1}{f-\Gamma}, \overline{\left(\frac{u'^2}{2} - \frac{1}{\sigma_0}\frac{\partial}{\partial p}\left(\frac{\bar{u}^2}{2}\right)\frac{\partial\phi'}{\partial p}\right)v}\right) + P_n\left(\frac{1}{f-\Gamma}, \overline{\bar{u}\beta u'}\right) + P_n\left(\frac{1}{f-\Gamma}, \overline{\bar{u}\gamma u'}\right) \tag{22b}$$

The true frequency cross-spectra are defined as the ensemble average of the sample frequency spectra. The frequency cross-spectra are estimated by a method similar to Bingham et al. (1967) which entails the following steps:

1. Removal of the annual cycle for the $N$ observations constituting the time series
2. Tapering of the first and the last 5% of resulting time series by multiplication of a segment of the cosine curve so that the ends of the series are zero
3. Adding back the annual cycle to the resulting time series
4. Performing a fast Fourier transform to obtain the $N$ harmonic coefficients
5. Calculation of the raw spectra using Eq. (18a). Consequently a running average over length $L$ is carried out. This averaging provides an estimate of the spectra through a rectangular spectral window of band width $(2L/N)f_N$, where $f_N$ is the Nyquist frequency.

The frequency spectra of the quadratic and triple products are inverse Fourier transformed on the time scale of 30–50 days to obtain their contribution to the total intraseasonal wave energy flux. The intraseasonal component of the linear variables, given in Eq. (17a), is filtered by using a first-order Butterworth filter. Therefore the total wave energy flux on the time scale of 30–50 days is obtained as the sum of the intraseasonal components of linear, quadratic and triple product terms.

Following the above method, we have calculated the wave energy flux using data sets for 8 years: 1987 through 1994. In Fig. 14, we show the latitude-time histories of these fluxes integrated zonally around the globe and vertically through the depth of the troposphere. In these illustrations the unshaded areas denote northward fluxes, whereas the shaded areas denote negative values, i.e. southward fluxes. Overall the panels 'a' through 'h' clearly show the emanation of the wave energy from the monsoonal latitudes towards the polar latitudes. Furthermore, a convergence of wave energy flux over the very high latitudes is evident from the change in the sense of propagation, i.e. south to north near 60°N, and in a reverse direction near the polar latitudes.

## 6. Concluding remarks

The zonal flow anomalies on the time scale of 30–50 days have large amplitudes in the extratropical upper troposphere of the middle latitudes. Monsoon activity on this time scale has been studied for well over 15 years by numerous investigators. It had been quite difficult to relate these intraseasonal activities of the tropical and extratropical latitudes because of the separation (critical latitude) of the tropical easterlies from the extratropical westerlies. The linear theory of wave energy flux precludes any direct communication across this barrier. One could think of an episodic opening of such a barrier during periods of extension of zonal flows beyond the mean critical latitude. However, we felt that there was a more general issue of wave energy flux that pertains to this non-linear problem in the frequency domain. We show that the assumption of a time mean zonal flow, which is inherent in the linear theory of wave energy flux, is not entirely valid on the Madden–Julian time scale. We have examined the zonally averaged zonal-flow anomalies over several years of data for the lower and the upper troposphere. We note that zonal-flow oscillations with amplitudes of the order of 1–3 m $s^{-1}$ prevail in the lower as well as the higher latitudes. Since zonal-flow anomalies on the time scale of the Madden–Julian oscillation exhibit a meridional motion, we can think of the critical latitude itself exhibiting a meridional motion for the non-linear problem. In the non-linear formulation of the wave energy flux these intraseasonal oscillations of the zonally averaged zonal flows are present and the non-linear theory accommodates the presence of meridional zonal-flow alterations.

We partitioned the expression for the non-linear wave energy flux into a number of linear, quadratic and triple product non-linearities. These were subjected to a formal computation in the frequency domain. This entailed the computation of co-spectra of the respective time series. By following methods originally proposed by Hayashi (1980) it was possible to obtain the latitude–time depictions of the meridional flux of the wave energy integrated over the depth of the atmosphere. Furthermore we clearly noted that there is a distinct continuity of these fluxes from the latitudes of the monsoons all the

way to the polar latitudes. This was based on 6 separate years of data analysis. The most important result of this study was the demonstration of the convergence of wave energy flux present at these polar latitudes; thus leading to the possibility that the polar maximum of the zonal-flow amplitudes on the intraseasonal time scales is indeed related to the monsoonal intraseasonal oscillation in the frequency domain.

This procedure holds promise for the examination of the interannual variability of the global aspects of the Madden–Julian oscillation. Furthermore the length of day issues on this time scale need to be viewed in the context of the angular momentum budget of the Earth–atmosphere system. Addressing such issues in the frequency domain would not only provide a better understanding of the tropical–middle latitude interaction on these time scales but can also be revealing of the entire cycle of angular momentum and the length of day variations on these time scales. This approach is fairly general and can be used to study tropical–middle latitude interactions in other frequency windows as well.

## Acknowledgements

This work was supported by NSF Grant Number ATM 9312537 and NOAA Grant No. NA56GP0013. The computations for this research were performed at the CRAY/YMP at NCAR which is sponsored by the National Science Foundation.

## Appendix A

Differentiating Eq. (15) with respect to pressure and rearranging, we get:

$$\frac{\partial}{\partial p}(\omega' u') = \frac{1}{\sigma_0}\frac{\partial}{\partial p}\left\{\left(\frac{2\bar{u}\tan\theta}{R}+f\right)\frac{\partial \bar{u}}{\partial p}v'u' - \frac{\partial}{\partial t}\left(\frac{\partial \phi'}{\partial p}\right)u' - \frac{\bar{u}u'}{R\cos\theta}\frac{\partial}{\partial\lambda}\left(\frac{\partial\phi'}{\partial p}\right) - \frac{u'2}{R\cos\theta}\frac{\partial}{\partial\lambda}\left(\frac{\partial\phi'}{\partial p}\right) - \frac{u'v'}{R\cos\theta}\frac{\partial}{\partial\theta}\left(\frac{\partial\phi'}{\partial p}\right)\right\} \tag{A1}$$

$\partial/\partial p(\bar{u}\omega')$ can be written as:

$$\frac{\partial}{\partial p}(\bar{u}\omega') = \omega'\frac{\partial\bar{u}}{\partial p} + \bar{u}\frac{\partial\omega'}{\partial p}$$

Substituting $\omega'$ from Eq. (15) and $\partial\omega'/\partial p$ from Eq. (12) in the above equation, we obtain

$$\frac{\partial(\bar{u}\omega')}{\partial p} = \left[\frac{1}{\sigma_0}\frac{\partial\bar{u}}{\partial p} - \frac{\partial}{\partial t}\left(\frac{\partial\phi'}{\partial p}\right) - \frac{\bar{u}}{R\cos\theta}\frac{\partial}{\partial\lambda}\left(\frac{\partial\phi'}{\partial p}\right) + v'\left(\frac{2\bar{u}\tan\theta}{R}+f\right)\frac{\partial\bar{u}}{\partial p} - \frac{\bar{u}}{R\cos\theta}\frac{\partial}{\partial\lambda}\left(\frac{\partial\phi'}{\partial p}\right) - \frac{v'}{R}\frac{\partial}{\partial\theta}\left(\frac{\partial\phi'}{\partial p}\right)\right] - \bar{u}\left[\frac{1}{R\cos\theta}\frac{\partial u'}{\partial\lambda} + \frac{1}{R\cos\theta}(v'\cos\theta)\right] \tag{A2}$$

Also,

$$\frac{\partial}{\partial p}(u'\omega') = \frac{1}{\sigma_0}\frac{\partial u'}{\partial p} - \frac{\partial}{\partial t}\left(\frac{\partial \phi'}{\partial p}\right) - \frac{\bar{u}}{R\cos\theta}\frac{\partial}{\partial \lambda}\left(\frac{\partial \phi'}{\partial p}\right) + v'\left(\frac{2\bar{u}}{R}\tan\theta + f\right)\frac{\partial \bar{u}}{\partial p} - \frac{u'}{R\cos\theta}\frac{\partial}{\partial \lambda}\left(\frac{\partial \phi'}{\partial p}\right) - \frac{v'}{R}\frac{\partial}{\partial \theta}\left(\frac{\partial \phi'}{\partial p}\right) - \frac{u'}{R\cos\theta}\frac{\partial u'}{\partial \lambda} - \frac{u'}{R\cos\theta}\frac{\partial}{\partial \theta}(v'\cos\theta) \tag{A3}$$

Substituting $\frac{\partial(\bar{u}\omega')}{\partial p}$ and $\frac{\partial(u'\omega')}{\partial p}$ from Eqs. (A2) and (A3), respectively, in Eq. (13), we obtain

$$\left[-f + \frac{1}{R\cos\theta}\frac{\partial}{\partial \theta} - (\bar{u}\cos\theta) + \left(\frac{2\bar{u}\tan\theta}{R} + f\right)\frac{1}{R}\frac{\partial}{\partial \theta}\frac{1}{\sigma_0}\left(\frac{\partial \bar{u}}{\partial p}\right)^2\right]v' + \frac{1}{R\cos\theta} \times \frac{\partial}{\partial \lambda}\left[\bar{u}u' + \phi' - \frac{1}{\sigma_0}\frac{\partial}{\partial p}\left(\frac{\bar{u}^2}{2}\right)\frac{\partial \phi'}{\partial p} + \frac{u'^2}{2}\right] + \left[\frac{\partial u'}{\partial t} - \frac{1}{\sigma_0}\frac{\partial \bar{u}}{\partial p}\frac{\partial}{\partial t}\left(\frac{\partial \phi'}{\partial p}\right)\right] - \frac{1}{\sigma_0}\frac{\partial u'}{\partial p}\cdot\frac{\bar{u}}{R\cos\theta}\frac{\partial}{\partial \lambda}\left(\frac{\partial \phi'}{\partial p}\right) - \frac{1}{\sigma_0}\frac{\partial u'}{\partial p}\cdot\frac{u'}{R\cos\theta}\frac{\partial}{\partial \lambda}\left(\frac{\partial \phi'}{\partial p}\right) + \left[\frac{1}{\sigma_0}\frac{\partial \bar{u}}{\partial p}\left(\frac{2\bar{u}}{R}\tan\theta + f\right)\frac{\partial u'}{\partial p} - \frac{1}{\sigma_0}\frac{\partial \bar{u}}{\partial p}\frac{1}{R}\frac{\partial}{\partial \theta}\left(\frac{\partial \phi'}{\partial p}\right) + \frac{1}{R\cos\theta}\frac{\partial}{\partial \theta}(u\cos\theta) - \frac{1}{\sigma_0}\frac{\partial u'}{\partial p}\frac{1}{R}\frac{\partial}{\partial \theta}\left(\frac{\partial \phi'}{\partial p}\right)\right]v' - \frac{1}{\sigma_0}\frac{\partial u'}{\partial p}\frac{\partial}{\partial t}\left(\frac{\partial \phi'}{\partial p}\right) = 0 \tag{A4}$$

Using the thermal wind relation in the above, we get

$$\left[-f + \frac{1}{R}\frac{\partial \bar{u}}{\partial \theta} - \left(\frac{\bar{u}\tan\theta}{R}\right) - \frac{1}{R}\frac{\partial}{\partial \theta}\left(\frac{\partial \bar{\phi}}{\partial p}\right)\left(\frac{1}{\sigma_0}\frac{\partial \bar{u}}{\partial p}\right)\right]v' + \frac{1}{R\cos\theta}\frac{\partial}{\partial \lambda} \times \left[\bar{u}u' + \phi' + \left\{\frac{u'^2}{2} - \frac{1}{\sigma_0}\frac{\partial}{\partial p}\left(\frac{\bar{u}^2}{2}\right)\frac{\partial \phi'}{\partial p}\right\}\right] + \left[\frac{\partial u'}{\partial t} - \frac{\partial}{\partial t}\left(\frac{\partial \bar{u}}{\sigma_0 \partial p}\frac{\partial \phi'}{\partial p}\right) - \frac{1}{\sigma_0}\frac{\partial}{\partial p}\frac{u'^2}{2}\frac{1}{R\cos\theta}\frac{\partial}{\partial \lambda}\left(\frac{\partial \phi'}{\partial p}\right)\right] + \left[\frac{1}{\sigma_0}\frac{\partial \bar{u}}{\partial p}\left(\frac{2\bar{u}}{R}\tan\theta + f\right)\frac{\partial u'}{\partial p} - \frac{1}{\sigma_0}\frac{\partial \bar{u}}{\partial p}\frac{1}{R}\frac{\partial}{\partial \theta}\left(\frac{\partial \phi'}{\partial p}\right) + \frac{1}{R\cos\theta}\frac{\partial}{\partial \theta}(\bar{u}\cos\theta) - \frac{1}{\sigma_0}\frac{\partial u'}{\partial p}\frac{1}{R}\frac{\partial}{\partial \theta}\left(\frac{\partial \phi'}{\partial p}\right)\right]v' - \frac{1}{\sigma_0}\frac{\partial u'}{\partial p}\frac{\partial}{\partial t}\left(\frac{\partial \phi'}{\partial p}\right) = 0 \tag{A5}$$

Writing,

$$\Gamma = \frac{1}{R}\frac{\partial \bar{u}}{\partial \theta} - \frac{\bar{u}\tan\theta}{R} - \frac{1}{R}\frac{\partial}{\partial\theta}\left(\frac{\partial\bar{\Phi}}{\partial p}\right)\left(\frac{1}{\sigma_0}\frac{\partial\bar{u}}{\partial p}\right)$$

$$\beta = \frac{\partial}{\partial t}\left[u' - \frac{1}{\sigma_0}\frac{\partial\bar{u}}{\partial p}\frac{\partial\Phi'}{\partial p}\right] - \frac{1}{\sigma_0}\frac{\partial}{\partial p}\left(\frac{u'^2}{2}\right)\cdot\frac{1}{R\cos\theta}\frac{\partial}{\partial\lambda}\left(\frac{\partial\Phi'}{\partial p}\right)$$

$$\gamma = \left\{\frac{1}{R\cos\theta}\frac{\partial}{\partial\theta}(\bar{u}\cos\theta) + \frac{1}{\sigma_0}\frac{\partial\bar{u}}{\partial p}\left(\frac{2\bar{u}}{R}+f\right)\frac{\partial u'}{\partial p}\right\}v'$$

$$-\left\{\frac{1}{\sigma_0}\frac{\partial\bar{u}}{\partial p}\cdot\frac{1}{R}\frac{\partial}{\partial\theta}\left(\frac{\partial\phi'}{\partial p}\right) + \frac{1}{\sigma_0}\frac{\partial u'}{\partial p}\cdot\frac{1}{R}\frac{\partial}{\partial\theta}\left(\frac{\partial\phi'}{\partial p}\right)\right\}v'$$

Eq. (A5) can be written as

$$-(f-\Gamma)v' + \frac{1}{R\cos\theta}\frac{\partial}{\partial\lambda}\left\{\bar{u}u' + \phi' + \frac{u'}{2} - \frac{1}{\sigma_0}\frac{\partial}{\partial p}\left(\frac{\bar{u}^2}{2}\right)\frac{\partial\phi'}{\partial p}\right\}$$

$$+\beta+\gamma-\frac{1}{\sigma_0}\frac{\partial u'}{\partial p}\frac{\partial}{\partial t}\left(\frac{\partial\phi'}{\partial p}\right) = 0$$

Multiplying Eq. (A5) by $[\bar{u}u' + \phi' + (u'/2) - (1/\sigma_0)(\partial/\partial p)(\bar{u}^2/2)(\partial\phi'/\partial p)]$ and averaging in the zonal direction ($\lambda$), we get

$$(f-\Gamma)\overline{\phi' v'} = \overline{\beta\phi'} + \overline{\left[\frac{u'^2}{2} - \frac{1}{\sigma_0}\frac{\partial}{\partial p}\left(\frac{\bar{u}^2}{2}\right)\frac{\partial\phi'}{\partial p}\right]\gamma} + \overline{\phi'\gamma}$$

$$-(f-\Gamma)\overline{\left\{\bar{u}\overline{u'v'} + v'\left[\frac{u'^2}{2} - \frac{1}{\sigma_0}\frac{\partial}{\partial p}\left(\frac{\bar{u}^2}{2}\right)\frac{\partial\phi'}{\partial p}\right]\right\}}$$

$$+\beta\overline{\left\{\bar{u}u' + \left[\frac{u'^2}{2} - \frac{1}{\sigma_0}\frac{\partial}{\partial p}\left(\frac{\bar{u}^2}{2}\right)\frac{\partial\phi'}{\partial p}\right]\right\}} + \overline{\bar{u}u'\gamma}$$

$$+\overline{\left\{\frac{-1}{\sigma_0}\frac{\partial u'}{\partial p}\frac{\partial}{\partial t}\left(\frac{\partial\phi'}{\partial p}\right)\right\}\left\{uu' + \phi' + \frac{u'^2}{2} - \frac{1}{\sigma_0}\frac{\partial}{\partial p}\left(\frac{\bar{u}^2}{2}\right)\frac{\partial\phi'}{\partial p}\right\}} \tag{A6}$$

Finally we obtain:

$$\overline{\phi' v'} = \frac{1}{(f-\Gamma)}\left[\overline{\beta\phi'}\left\{\frac{u'^2}{2} - \frac{1}{\sigma_0}\frac{\partial}{\partial p}\left(\frac{\bar{u}^2}{2}\right)\frac{\partial\phi'}{\partial p}\right\}\gamma\right]$$

$$+\frac{1}{(f-\Gamma)}\left(\overline{\phi'\gamma} - \bar{u}\left(\overline{\beta u'} + \overline{\gamma u'}\right)\right)\overline{\frac{1}{\sigma_0}\frac{1}{f-\Gamma}\frac{\partial u'}{\partial p}\left(\frac{\bar{u}^2}{2}\right)\frac{\partial\phi'}{\partial p}}$$

$$+\frac{1}{f-\Gamma}\overline{\left((\beta+\gamma)\frac{u'^2}{2}-\frac{1}{\sigma_0}\frac{\partial}{\partial p}\left(\frac{\bar{u}^2}{2}\right)\frac{\partial\phi'}{\partial p}\right)}$$

$$-\left(\overline{\bar{u}u'v'}+\overline{\left(\frac{u'^2}{2}-\frac{1}{\sigma_0}\frac{\partial}{\partial p}\left(\frac{\bar{u}^2}{2}\right)\frac{\partial\phi'}{\partial p}\right)v'}\right)$$

## References


Bingham, C., Godfrey, M.D., Tukey, J.W., 1967. Modern techniques of power spectrum estimation. IEEE Trans. Audio Electroacoustics AU-15, 56–66.

Comeaux, J., 1991. Origin and structure of the low frequency modes. M.S. Thesis, Department of Meteorology, Florida State University, Tallahassee, FL.

Eliassen, A., Palm, E., 1961. On the transfer of energy in stationary mountain waves. Geof. Pub. 3, 1–23.

Eliasen, E., Machenhauer, B., Rasmussen, E., 1970. On a numerical method of integration of hydrodynamical equations with a spectral representation of horizontal fields. Report No. 2, Institute of Theoretical Meteorology, University of Copenhagen, Denmark, 35 pp.

Goirala, R.M., Krishnamurti, T.N., 1992. Rain rates based on SSM/I, OLR and raingauge data sets. J. Met. Atmos. Phys. 50, 165–174.

Hayashi, 1980. Estimation of nonlinear energy transfer spectra by the cross-spectral method. J. Atmos. Sci., 37, 299–307.

Hendon, H.H., Liebmann, B., 1990. The intraseasonal (30–50 day) oscillation of the Australian summer monsoon. J. Atmos. Sci. 47, 2909–2923.

Jenkins, G.M., Watts, D.G., 1968. Spectral Analysis and its Applications. Holden-Day, 525 pp.

Krishnamurti, T.N., Subramaniam, M., Oosterhof, D.K. and Daughenbaugh, G., 1990. Predictability of low frequency modes. J. Met. Atmos. Phys. 44, 63–84.

Krishnamurti, T.N., Gadgil, S., 1985. On the structure of the 30 to 50 day mode over the globe during FGGE. Tellus 37A, 336–360.

Krishnamurti, T.N., Subramaniam, M., Oosterhof, D.K., Daughenbaugh, G., Xue, J., 1992a. One-month forecasts of wet and dry spells of the monsoon. Mon. Weather Rev. 120, 1191–1223.

Krishnamurti, T.N., Sinha, M.C., Krishnamurti, R., Oosterhof, D., Comeaux, J., 1992b. Angular momentum, length of day and monsoonal low frequency mode. J. Meteor. Soc. Japan, 1992, 131–165.

Krishnamurti, T.N., Han, S.-O., Misra, V., 1995. Prediction of the dry and wet spell of the Australian monsoon. Int. J. Climatol. 15, 753–771.

Orzag, S.A., 1970. Transform method for calculation of vector coupled sums. Application to the spectral form of the vorticity equation. J. Atmos. Sci. 27, 890–895.

Yanai, M., Lu, M.-M., 1983. Equatorially trapped waves at the 200 mb level and their association with convergence of wave energy flux. J. Atmos. Sci. 40, 2785–2803.

Zangvil, A., 1977. On the presentation and interpretation of spectra of large scale disturbances. Mon. Weather Rev. 105, 1469–1472.